AEM
Journals.ASM.org

Carbohydrate Catabolism in *Phaeobacter inhibens* DSM 17395, a Member of the Marine *Roseobacter* Clade

Katharina Wiegmann,[a] Michael Hensler,[b] Lars Wöhlbrand,[a] Marcus Ulbrich,[b] Dietmar Schomburg,[b] Ralf Rabus[a,c]

Institute for Chemistry and Biology of the Marine Environment (ICBM), Carl von Ossietzky University Oldenburg, Oldenburg, Germany[a]; Institute for Biochemistry, Biotechnology and Bioinformatics, Technische Universität Carolo-Wilhelmina Braunschweig, Braunschweig, Germany[b]; Max Planck Institute for Marine Microbiology, Bremen, Germany[c]

Since genome analysis did not allow unambiguous reconstruction of transport, catabolism, and substrate-specific regulation for several important carbohydrates in *Phaeobacter inhibens* DSM 17395, proteomic and metabolomic analyses of *N*-acetylglucosamine-, mannitol-, sucrose-, glucose-, and xylose-grown cells were carried out to close this knowledge gap. These carbohydrates can pass through the outer membrane via porins identified in the outer membrane fraction. For transport across the cytoplasmic membrane, carbohydrate-specific ABC transport systems were identified. Their coding genes mostly colocalize with the respective "catabolic" and "regulatory" genes. The degradation of *N*-acetylglucosamine proceeds via *N*-acetylglucosamine-6-phosphate and glucosamine-6-phosphate directly to fructose-6-phosphate; two of the three enzymes involved were newly predicted and identified. Mannitol is catabolized via fructose, sucrose via fructose and glucose, glucose via glucose-6-phosphate, and xylose via xylulose-5-phosphate. Of the 30 proteins predicted to be involved in uptake, regulation, and degradation, 28 were identified by proteomics and 19 were assigned to their respective functions for the first time. The peripheral degradation pathways feed into the Entner-Doudoroff (ED) pathway, which is connected to the lower branch of the Embden-Meyerhof-Parnas (EMP) pathway. The enzyme constituents of these pathways displayed higher abundances in *P. inhibens* DSM 17395 cells grown with any of the five carbohydrates tested than in succinate-grown cells. Conversely, gluconeogenesis is turned on during succinate utilization. While tricarboxylic acid (TCA) cycle proteins remained mainly unchanged, the abundance profiles of their metabolites reflected the differing growth rates achieved with the different substrates tested. Homologs of the 74 genes involved in the reconstructed catabolic pathways and central metabolism are present in various *Roseobacter* clade members.

Carbohydrates are important constituents of the global carbon cycle. In marine surface waters they can account for about 21% of the dissolved organic carbon and reach concentrations of 7 to 33 μM (1). Although polysaccharides are dominant, monosaccharides have also been detected in the Atlantic, Pacific, and Antarctic Oceans at an average concentration of 4.3 μM (1). A prominent monosaccharide is *N*-acetylglucosamine, which is the monomer of chitin, the second most abundant polymer in the environment. Chitin is the key component of fungal cell walls, is present in the exoskeletons of worms, molluscs, and arthropods (2), and is estimated to account for about 10% of marine bacterial production (3). Another important source of *N*-acetylglucosamine is the peptidoglycan of the Gram-negative bacterial cell wall (4). Glucosamine (including deacetylated *N*-acetylglucosamine) has been detected as the most abundant amino sugar in marine surface waters (17 to 56 nM), with higher prevalences in the Atlantic and Pacific Oceans than in the Arctic Ocean (4). Glucose, on the other hand, is the most abundant neutral monosaccharide, with concentrations as high as 15 to 65 nM in the equatorial Pacific, where it accounts for 15 to 47% of bacterial production (5). Other abundant aldoses in seawater are galactose, mannose, and xylose (6). In addition to neutral monosaccharides and amino sugars, disaccharides and sugar alcohols are noteworthy carbohydrate species. One representative of the latter is mannitol, which acts as a "compatible solute" in algae (7). In general, the most abundant disaccharide in the environment is sucrose, due to its formation by photosynthesis in higher plants (8).

The carbohydrates in the marine water column are utilized predominantly by heterotrophic bacteria. A recent survey of transporter gene occurrence in coastal bacterioplankton communities revealed that *Roseobacter* clade members have the highest number of carbohydrate-associated transporter genes (9). This is in accord with the finding that roseobacters, as well as SAR11 affiliates, contribute significantly to glucose uptake in coastal North Sea waters (10). The striking dominance of the alphaproteobacterial *Roseobacter* clade among marine bacterioplankton members is paralleled by the wide range of metabolic capacities of its members (11). Due to this biogeographical prominence and ecophysiological relevance, more than 75 roseobacter genomes have been sequenced to date. Among them is that of *Phaeobacter inhibens* DSM 17395 (12), which was recently reclassified from *Phaeobacter gallaeciensis* DSM 17395 (13). *Phaeobacter* species are globally distributed in the marine system, e.g., in sediments of the Arctic Ocean (14), the Yellow Sea (15), and the Mediterranean Sea (16), and in surface water of the German Wadden Sea (17). Furthermore, they are constituents of marine biofilms (18) and are associated with scallops (19) and algae (12). The main physiological characteristics of *P. inhibens* DSM 17395 are the formation of the antibiotic tropodithietic acid (20) and its nutritional versatility

Received 1 March 2014 **Accepted** 15 May 2014
Published ahead of print 23 May 2014
Editor: F. E. Löffler
Address correspondence to Ralf Rabus, rabus@icbm.de.
Supplemental material for this article may be found at http://dx.doi.org/10.1128/AEM.00719-14.

doi:10.1128/AEM.00719-14

(carbohydrates, organic acids, and all 20 proteinogenic amino acids [21]). Due to these characteristics, *P. inhibens* DSM 17395 was selected as a systems biology model for studying the molecular basis of the habitat success of heterotrophic roseobacters. An initial proteomic/metabolomic study with *P. inhibens* DSM 17395 demonstrated that its central metabolism was unaffected by the growth phase (22). Furthermore, the Entner-Doudoroff (ED) pathway was identified as the key route for glucose breakdown across roseobacters (22, 23). During growth with complex Marine Broth (MB) as a surrogate for the complex nutritional conditions typically resulting from the collapse of algal blooms, *P. inhibens* DSM 17395 simultaneously degraded various amino acids and other substrates (24). A subsequent time-resolved study revealed differing degrees of substrate preferences (high to low) during growth with Casamino Acids, containing 15 different detectable amino acids (25). Genomically unclear degradation pathways of nine amino acids could be elucidated by combined proteomics, enzymatics, and metabolomics and could be shown by comparative genomics to be archetypical for roseobacters (26). Besides amino acids, carbohydrates are common substrates for *P. inhibens* DSM 17395, but their catabolism has not been investigated so far. In the present study, the uptake and degradation of five representative carbohydrates were studied by combined proteomic and metabolomic analyses, and their dissemination across roseobacters and other marine heterotrophic bacteria was studied by comparative genomics.

MATERIALS AND METHODS

Cultivation. *Phaeobacter inhibens* DSM 17395 was obtained from the Deutsche Sammlung von Mikroorganismen und Zellkulturen GmbH (DSMZ; Braunschweig, Germany) and since then has been maintained in our laboratory.

The range of utilizable carbohydrates was assessed by incubating *P. inhibens* DSM 17395 in glass tubes filled with 5 ml defined mineral seawater medium (SWM) (22) supplemented with 1 of 18 different carbohydrates at 1 mg ml^{-1} (3 to 7 mM). Freshly grown precultures in rich (MB) medium were washed with substrate-free SWM prior to inoculation of carbohydrate-containing SWM. Test cultures were incubated on a rotary shaker at 28°C. Growth was monitored by measuring the optical density at 600 nm (OD_{600}). Thirteen of the 18 carbohydrates investigated allowed growth (see Table S1 in the supplemental material).

For further analyses five growth substrates, representing different classes of carbohydrates, were selected: *N*-acetylglucosamine (5 mM), mannitol (5 mM), sucrose (2.5 mM), glucose (5 mM), and xylose (5 mM). Furthermore, succinate (20 mM) served as a reference. For substrate adaptation, *P. inhibens* DSM 17395 was grown with each substrate for 5 passages in Erlenmeyer flasks and was then stored in glycerol stocks, as described recently (26).

For each of the metabolomic and proteomic analyses, 12 replicate cell pellets (~100 mg [wet weight]) were generated per substrate condition. Starting from a glycerol stock, 3 passages were conducted before six main cultures (250 ml) were inoculated with 2% [vol/vol] preculture (25). At half-maximal optical density (½ OD_{max}), 20 ml of each main culture was further incubated in 100-ml Erlenmeyer flasks (see Fig. S1 in the supplemental material), and the remainder was harvested as described previously (22), except for cell pellets allocated for metabolomics, which were washed with 3.7% (wt/vol) NaCl. The substrate-specific ½ OD_{max} values and corresponding protein contents were as follows: for succinate, an OD_{600} of 1.41 and 76.3 mg protein $liter^{-1}$; for *N*-acetylglucosamine, an OD_{600} of 0.55 and 31.4 mg protein $liter^{-1}$; for mannitol, an OD_{600} of 0.70 and 23.7 mg protein $liter^{-1}$; for sucrose, an OD_{600} of 0.52 and 18.4 mg protein $liter^{-1}$; for glucose, an OD_{600} of 0.48 and 25.2 mg protein $liter^{-1}$; and for xylose, an OD_{600} of 0.46 and 18.3 mg protein $liter^{-1}$. For sucrose- and succinate-grown cells, two additional main cultures were harvested for RNA isolation and subsequent reverse transcriptase PCR (RT-PCR). Cultures were harvested as described above. The resulting cell pellets were resuspended in 1.5 ml RNAprotect Bacteria reagent (Qiagen, Hilden, Germany) and were incubated for 10 min at room temperature prior to centrifugation and storage at −80°C.

All cultivation steps were purity controlled by microscopy (Axiostar; Zeiss AG, Göttingen, Germany) and plating on MB agar.

Proteomics. (i) Analysis of soluble proteome by 2D-DIGE and matrix-assisted laser desorption ionization–time of flight (MALDI-TOF) tandem mass spectrometry (MS-MS). For 2-dimensional difference in gel electrophoresis (2D-DIGE) analysis, cell pellets of three biological replicates for each substrate condition were resuspended in lysis buffer {7 M urea, 2 M thiourea, 30 mM Tris-HCl, 4% 3-[(3-cholamidopropyl)-dimethylammonio]-1-propanesulfonate [CHAPS] [final pH 8.5]}, and cells were disrupted using the Plus One Sample Grinding kit (GE Healthcare, Munich, Germany) as described previously (27, 28). The protein content was determined by the method described by Bradford (29). Before electrophoresis, proteins were covalently labeled with CyDye DIGE Fluor dyes (GE Healthcare) essentially as reported previously (28). For each sample, 50 μg protein was labeled with 200 pmol of either Cy3 (for each of the five test states [carbohydrate-grown cells]), Cy5 (for the reference state [succinate-grown cells]), or Cy2 (for the internal standard [equal amounts of all test state samples and the reference state sample]). Then each labeled test state sample was mixed with the reference state sample and the internal standard, and the mixture was transferred to 24-cm-long, nonlinear (NL) immobilized pH gradient (IPG) strips with pH ranges from 3 to 5.6 and from 3 to 11 (GE Healthcare) for 1st-dimension separation. Isoelectric focusing, reduction, alkylation, and 2nd-dimension separation according to molecular mass by SDS-PAGE were carried out as described previously (22). After the completion of electrophoresis, 2-dimensional electrophoresis (2DE) gels were immediately scanned with a Typhoon 9400 scanner (GE Healthcare). Using DeCyder software (version 7.0; GE Healthcare), images were cropped and analyzed in two separate work packages according to the different pH gradients applied (pH 3 to 5.6 NL and pH 5 to 11 NL). The detection parameters were set as described previously (30). Those protein spots that changed in abundance by $\geq|1.5|$-fold, matched in at least 75% of the gels analyzed, and had *P* values of <0.05 by analysis of variance (ANOVA) and *t* test values of $<10^{-4}$ were regarded as significantly regulated (31).

For protein identification, separate replicate 2DE gels with 300-μg protein loads were run for each substrate condition and were stained with colloidal Coomassie brilliant blue (cCBB) after electrophoresis (30). Differentially abundant protein spots were excised with the EXQuest spot cutter (Bio-Rad, Munich, Germany). As described recently (24), excised protein spots were first washed and digested and were then spotted onto AnchorChip steel targets (Bruker Daltonik GmbH, Bremen, Germany) and subjected to mass spectrometric analysis with an UltrafleXtreme MALDI–two-stage TOF (TOF-TOF) mass spectrometer (Bruker Daltonik GmbH). Peptide mass fingerprint (PMF) searches and MS-MS searches were performed with a Mascot server (version 2.3; Matrix Science, London, United Kingdom) and the ProteinScape platform (version 3.0; Bruker Daltonik GmbH) as described previously (26).

(ii) Analysis of proteins from the cytoplasmic and outer membrane protein-enriched fractions by nano-liquid chromatography (nano-LC)-ESI-MS-MS. Cytoplasmic and outer membrane proteins from two biological replicates per substrate condition were prepared via sequential solubilization with sarcosyl and SDS essentially as described recently (32). Outer membrane-enriched (2.5 μg) and cytoplasmic membrane-enriched (4.0 μg) protein fractions were separated according to molecular mass on 7-cm-long, 1-mm-thick 12.5% SDS-PAGE gels. Four slices per gel lane were cut into smaller pieces and were subjected to in-gel-digestion as described previously (32). The tryptic peptides generated were separated with an UltiMate 3000 RSLCnano system (Thermo Fisher Scientific, Germering, Germany) equipped with a trap column (PepMap C_{18} Nano-

Trap column; pore size, 100 Å; bead size, 3 μm; inner diameter, 75 μm; length, 2 cm; Thermo Fisher Scientific) and a 15-cm analytical column (C_{18}; pore size, 100 Å; bead size, 2 μm; inner diameter, 75 μm; length, 15 cm; Thermo Fisher Scientific). The following linear gradient of increasing acetonitrile concentrations was applied using solvent A (0.1% trifluoroacetic acid [TFA]) and solvent B (80% acetonitrile, 0.1% TFA): 0 to 12 min, 4% B; 12 to 120 min, 4 to 50% B; 120 to 130 min, 50 to 95% B; 130 to 135 min, 95% B. The eluent was continuously analyzed by an online coupled electrospray ionization (ESI) ion trap mass spectrometer (amaZon ETD; Bruker Daltonik GmbH) operated as described previously (24). Protein identification was performed with ProteinScape (version 3.1) on a Mascot server (version 2.3) against the translated genome sequence of *P. inhibens* DSM 17395 (12) by applying a target-decoy strategy and a false discovery rate of <1.0% (24).

(iii) Shotgun proteomics by nano-LC-ESI-MS-MS. For shotgun proteomic analysis, cell pellets were resuspended in 200 μl lysis buffer (7 M urea, 2 M thiourea, 30 mM Tris-HCl [final pH 8.5]) and were disrupted by means of the Sample Grinding kit (GE Healthcare). Fifty micrograms of total protein was subjected to reduction and alkylation using 45 mM dithiothreitol (DTT) and 100 mM iodoacetamide, respectively, prior to tryptic digestion overnight (1 μg enzyme). Peptides were separated with an UltiMate 3000 RSLCnano system (Thermo Fisher Scientific) with a trap column setup (see above) on a 25-cm analytical column (C_{18}; pore size, 100 Å; bead size, 2 μm; inner diameter, 75 μm; length, 25 cm; Thermo Fisher Scientific) by applying the following gradient: 0 to 12 min, 4% B; 12 to 255 min, 4 to 50% B; 255 to 270 min, 50 to 95% B; 270 to 275 min, 95% B. Protein identification was performed with ProteinScape on a Mascot server (see above for details). The peptide data of all three biological replicates were compiled, and only proteins identified with 2 or more peptides were accepted.

Metabolomic analyses. Intracellular metabolites were extracted as described previously (22), except that for resuspension of the cell pellets, 1.5 ml ethanol containing 30 μl ribitol (0.2 mg ml^{-1}) was used. Furthermore, after phase separation, 1 ml of the upper polar phase was transferred to a 2-ml reaction tube and was dried in a vacuum concentrator for gas chromatography (GC)-MS analysis. The two-step derivatization reaction was performed essentially as described previously (25).

Intracellular metabolites were analyzed by GC-MS as described previously (26) using a Leco Pegasus 4D GC×GC-TOF MS (Leco Instrumente, Mönchengladbach, Germany) operated in GC-TOF mode and equipped with an MPS 2 XL autosampler (Gerstel, Mülheim an der Ruhr, Germany). The solvent delay time was adjusted to 278 s, and the detector voltage was set to 1,750 V.

Additionally, the samples were analyzed using the JMS-T100GC AccuTOF GC (JEOL GmbH, Eching, Germany), equipped with an MPS 2 Twister autosampler (Gerstel). Tuning with perfluorokerosene (MassCom, Bremen, Germany) was carried out according to the manufacturer's instructions. Samples (1 μl) were injected in splitless mode into a programmed-temperature vaporizer (PTV) injector (Gerstel), equipped with a 71- by 1-mm CIS 4 glass liner filled with silanized glass wool (Gerstel). After an initial time of 0.02 min at 70°C, the temperature was increased at 12°C s^{-1} to 330°C, followed by holding at 330°C for 5 min. Gas chromatography was performed with a 6890N Agilent GC (Agilent Technologies, Waldbronn, Germany) equipped with a ZB-5MS column (length, 30 m; inner diameter, 0.25 mm; particle size, 25 μm; Phenomenex, Aschaffenburg, Germany). The helium flow was set to a constant 1.2 ml min^{-1}. After 1 min at 70°C, the GC oven temperature was increased to 330°C at 10°C min^{-1}, followed by an additional constant temperature period at 330°C for 3 min. The transfer line temperature was set to 250°C. The electron impact mode at 70 eV was used for ionization; the ion source temperature was set to 200°C, the detector voltage to 2,400 V, and the emission current to 300 μA. After 3.8 min (solvent delay time), full-scan mass spectra were collected from *m/z* 45 to 600 at 5 scans s^{-1} with MassCenter Main software (version 2.3.0.1; JEOL).

Data were analyzed as described recently (25, 26). The internal standard ribitol and the cell mass were used for normalization, and finally, data were centralized to the reference state succinate-grown cells.

RNA isolation and RT-PCR. The primers (purchased from biomers.net, Ulm, Germany) designed for α-glucosidase (encoded by *algA*) (*algA*_F [5′-TGCTGTCGCATACCTCTGAC-3′] and *algA*_R [5′-GTATCAAGG CGAAAGCCATC-3′]) resulted in a theoretical PCR product of 304 bp. For RNA isolation, two biological replicates (100 mg each) of sucrose- and succinate-grown cell pellets were used (for harvest, see above). RNA was isolated as described previously (33) by using acidic phenol and PCI (phenol-chloroform-isoamyl alcohol, 25:24:1), followed by washing with ethanol. Then DNA was digested with DNase I (34). The completeness of the digestion was verified via PCR employing primers *aglA*_R and *aglA*_F.

For reverse transcription, the final mixture consisted of 2.5 μg RNA (isolated from sucrose- or succinate-grown cells), 1.0 μl deoxynucleoside triphosphates (dNTPs) (10 mM), 2.0 μl antisense primer (10 μM) (*aglA*_R), 4.0 μl RT buffer, 1.0 μl H Minus Moloney murine leukemia virus (M-MuLV) reverse transcriptase (200 U μl^{-1}; MBI Fermentas, St. Leon-Roth, Germany), and PCR-H_2O (to 20 μl). The reverse transcription took place at 42°C for 60 min.

Then a PCR was performed, the products of which were separated on a 1.5% agarose gel. For this purpose, 2 μl of *aglA* cDNA, RNA, or PCR-H_2O (negative control), or 1 μl of *P. inhibens* DSM 17395 DNA (positive control), was used as the template. Furthermore, 0.4 μl of the forward and reverse primers, 10 μl 2× PCR master mix (Promega, Madison, WI, USA), and PCR-H_2O (to 20 μl) were added. The PCR program for amplification of *aglA* was as follows: 94°C for 10 min; 39 cycles of 94°C for 30 s, 60°C for 1 min, and 72°C for 2.5 min; 72°C for 5 min; and 4°C for 30 s.

BigDye sequencing (Applied Biosystems, Foster City, CA, USA) revealed the identities of the PCR products.

Genome-based metabolic reconstruction. Carbohydrate degradation pathways were reconstructed based on the sequenced and annotated genome of *P. inhibens* DSM 17395 (12) and reanalysis using MetaCyc (35), KEGG (36), Artemis (version 10.0) (37), and BLASTP (38).

For two reaction steps in the degradation of *N*-acetylglucosamine, no enzymes were predicted based on the genome of *P. inhibens* DSM 17395. To search for enzyme candidates, hidden Markov models (HMMs) (39) were used. Pretrained HMMs were taken from TIGRFAMs (http://www.jcvi.org/cgi-bin/tigrfams/index.cgi) if provided. Otherwise, an HMM was trained by collecting the sequence data of manually annotated enzymes for the required EC number obtained from the Braunschweig Enzyme Database (BRENDA) (40) and UniProt (41). The sequences collected were aligned by using Clustal Omega with standard settings (42, 43). After this, HMMBuild and finally HMMSearch were used to search candidates for the required enzymes in *P. inhibens* DSM 17395.

Comparative genomics. The *P. inhibens* DSM 17395 genome, 27 other genomes from *Roseobacter* clade members, and genomes of 4 additional representatives of non-*Roseobacter Rhodobacterales* were collected from the National Center for Biotechnology Information (NCBI) proteome database (ftp://ftp.ncbi.nlm.nih.gov/genomes/Bacteria) (38). In addition, a selection of 30 other *Proteobacteria* and *Bacteroidetes* (*Flavobacteria*) was chosen in order to compare the genomes of marine heterotrophic bacteria lying outside the *Rhodobacteraceae*.

The predicted proteomes assembled in FASTA format were used to group orthologous/paralogous protein sequences across the genomes analyzed with the OrthoMCL algorithm, version 2.0.9 (44). The all-versus-all-BLASTP phase was carried out by BLAST, version 2.2.28+ (45). After the OrthoMCL software was run with standard parameters for bacteria (threshold for ortholog determination, an E value of $\leq 10^{-4}$ and an identity of ≥50%), the results were loaded into a relational database based on MySQL. Furthermore, the ortholog data were adjusted and supplemented by the "Genome Gene Best Homologs/Orthologous" service of the Integrated Microbial Genomes (IMG) database and comparative analysis system (46). Orthologous genes in the genomes of the 62 organisms tested were identified as bidirectional best BLAST hits with an E value below 10^{-4} and an identity higher than 50%. Since these criteria for the identi-

fication of orthologs were rather strict, and the same enzymatic activity can be performed by proteins with different sequences, an additional search for the presence of isofunctional enzymes was carried out in the EnzymeDetector website. The criteria for enzyme function prediction described in reference 47 were applied.

Information about additional gene loci in the *P. inhibens* DSM 17395 genome annotated with an identical EC number and an identical or better EnzymeDetector score was obtained from the EnzymeDetector website (47) and was integrated.

The information collected was analyzed with respect to the presence of orthologous genes, their genomic contexts, and their predicted enzyme functions. If two or more genes were in close proximity, the gene cluster was classified into six different categories of relatedness as reported previously (26). Predicted isofunctional enzymes that do not meet the strict criteria for orthologs are indicated by an additional color in Fig. 2 (see also Fig. S7 in the supplemental material).

The synteny of the genomes compared and the rRNA tree representing the phylogenetic taxonomy of *Rhodobacterales* have been determined previously (26).

RESULTS AND DISCUSSION

Phaeobacter inhibens DSM 17395 is currently known to utilize 13 different carbohydrates as sole sources of carbon and energy for growth (see Table S1 in the supplemental material). Five of these carbohydrates, which are environmentally relevant and represent different chemical compound classes, were selected for this study: *N*-acetylglucosamine (amino sugar), mannitol (sugar alcohol), sucrose (disaccharide), glucose (hexose), and xylose (pentose). A combination of differential proteomics and metabolomics allowed the reconstruction of the uptake and catabolic routes for these five carbohydrates. The catabolic network, together with the genomic locations of the genes involved, is schematically drawn in Fig. 1, and dissemination across the *Roseobacter* clade is shown in Fig. 2.

Growth physiology. *P. inhibens* DSM 17395 was cultivated in defined mineral seawater medium containing one of the five selected carbohydrates (5 mM each, except for sucrose [2.5 mM]) or succinate (20 mM) (see Fig. S1 in the supplemental material). Since a higher concentration of succinate was applied, the highest maximal optical density (OD_{max}) of 2.4 was observed with this substrate. The sugars tested yielded OD_{max} values of 1.1 to 1.2, except for xylose (OD_{max}, 0.7), which, as a pentose, contains the fewest carbon atoms. The highest maximal specific growth rates (μ_{max}) were observed with cultures growing with succinate (0.22 h^{-1}) or *N*-acetylglucosamine (0.20 h^{-1}). The optimization of *P. inhibens* DSM 17395 to fast growth with *N*-acetylglucosamine agrees with the fact that this compound represents one of the most abundant carbohydrates in marine habitats (4). Growth with glucose (μ_{max}, 0.12 h^{-1}) or xylose (μ_{max}, 0.11 h^{-1}) was about half as fast. With mannitol and sucrose, considerably lower μ_{max} were achieved (0.04 and 0.02 h^{-1}, respectively). The observed mean μ_{max} value (0.10 h^{-1}) is in the same range as that previously observed with a variety of amino acids (on average, 0.11 h^{-1}) (26). A slightly higher μ_{max} of 0.17 h^{-1} was reached by cultures of *P. inhibens* DSM 17395 growing with Casamino Acids (25). The fastest growth of *P. inhibens* DSM 17395 is currently known for cultures in complex Marine Broth (MB) containing peptone and yeast extract (μ_{max}, 0.36 h^{-1}) (24).

Passage through the outer membrane. In Gram-negative bacteria, compounds have to traverse the outer membrane prior to entering the periplasm. Passage of smaller hydrophilic molecules (up to ~550 Da) occurs via facilitated diffusion mediated by membrane channels, so-called porins (48). To identify these in *P. inhibens* DSM 17395, a recently established method for the isolation of outer membrane protein-enriched fractions (32) was applied. By this method, seven outer membrane proteins could be identified (Fig. 3). One of them, protein c06130, is a predicted OmpA-like porin, as known from *Escherichia coli* K-12 (49, 50), and was detected under all substrate conditions studied. In contrast, the outer membrane protein c10290 was specifically identified in *N*-acetylglucosamine-grown cells, whereas plasmid-encoded protein 78p00530 was found under the other substrate conditions. This may imply that some outer membrane proteins could serve substrate-specific functions.

Carbohydrate transport and degradation pathways. (i) *N*-Acetylglucosamine degradation. The amino sugar *N*-acetylglucosamine is apparently transported into the cytoplasm via a specifically formed ATP-binding cassette (ABC) transporter, c27930 to c27970 (Fig. 1A and 3), reannotated as the *N*-acetylglucosamine ABC transport system (see Table S3 in the supplemental material).

As in *Xanthomonas campestris* pv. campestris (51), *N*-acetylglucosamine in *P. inhibens* DSM 17395 is degraded to fructose-6-phosphate via three steps (see Fig. S2 in the supplemental material). Two steps could not be reconstructed based on the original genome annotation but could be resolved via differential proteomics and metabolomics. In the first step, intracellularly detected *N*-acetylglucosamine (Fig. 4) is phosphorylated to *N*-acetylglucosamine-6-phosphate. This reaction is generally known to be performed by *N*-acetylglucosamine kinase (NagK). A BLAST search (homology to an *N*-acetylglucosamine kinase from *Roseobacter denitrificans* OCh 114; E value, 2e−48) and an HMM search (E value, 6e−30), as well as specific identification in *N*-acetylglucosamine-grown cells of *P. inhibens* DSM 17395, suggest that protein c27910 functions as NagK. In the second step, *N*-acetylglucosamine-6-phosphate deacetylase (NagA) cleaves off acetate, forming the detected metabolite glucosamine-6-phosphate. Acetyl coenzyme A (acetyl-CoA) synthetase activates the acetate for funneling into the TCA cycle or into lipid or amino acid biosynthesis (Fig. 1A; see also Table S4 in the supplemental material). In the third step, glucosamine-6-phosphate is isomerized and deaminated to fructose-6-phosphate. This transformation is proposed to be performed by protein c27890, which was 15.6-fold more abundant in *N*-acetylglucosamine-grown cells than in succinate-grown cells and was reannotated as glucosamine-6-phosphate deaminase (NagB; EC 3.5.99.6). Although protein c27890 is also similar to glucosamine-fructose-6-phosphate aminotransferase (GlmS; EC 2.6.1.16), its substrate-specific formation supports its proposed role in glucosamine-6-phosphate degradation (Fig. 3). In accord with such an assumption is the general function of the deaminase in the catabolic direction (2, 51, 52), whereas the activity of the biosynthetic transaminase is known from *E. coli* to be irreversible (53).

The *nagKBA* genes are arranged in an operon-like structure on the chromosome of *P. inhibens* DSM 17395 (Fig. 1B), agreeing with their functions proposed above. In juxtaposition to *nagKBA* on the opposite strand are *c27930* to *c27970*, encoding the above-mentioned ABC transporter. Between *nagKBA* and *c27930* to *c27970*, *murQ* codes for *N*-acetylmuramate-6-phosphate etherase. MurQ (4.0-fold more abundant in *N*-acetylglucosamine-grown cells than in succinate-grown cells) converts *N*-acetylglucosamine-6-phosphate to *N*-acetylmuramate-6-phosphate; in their dephospho-

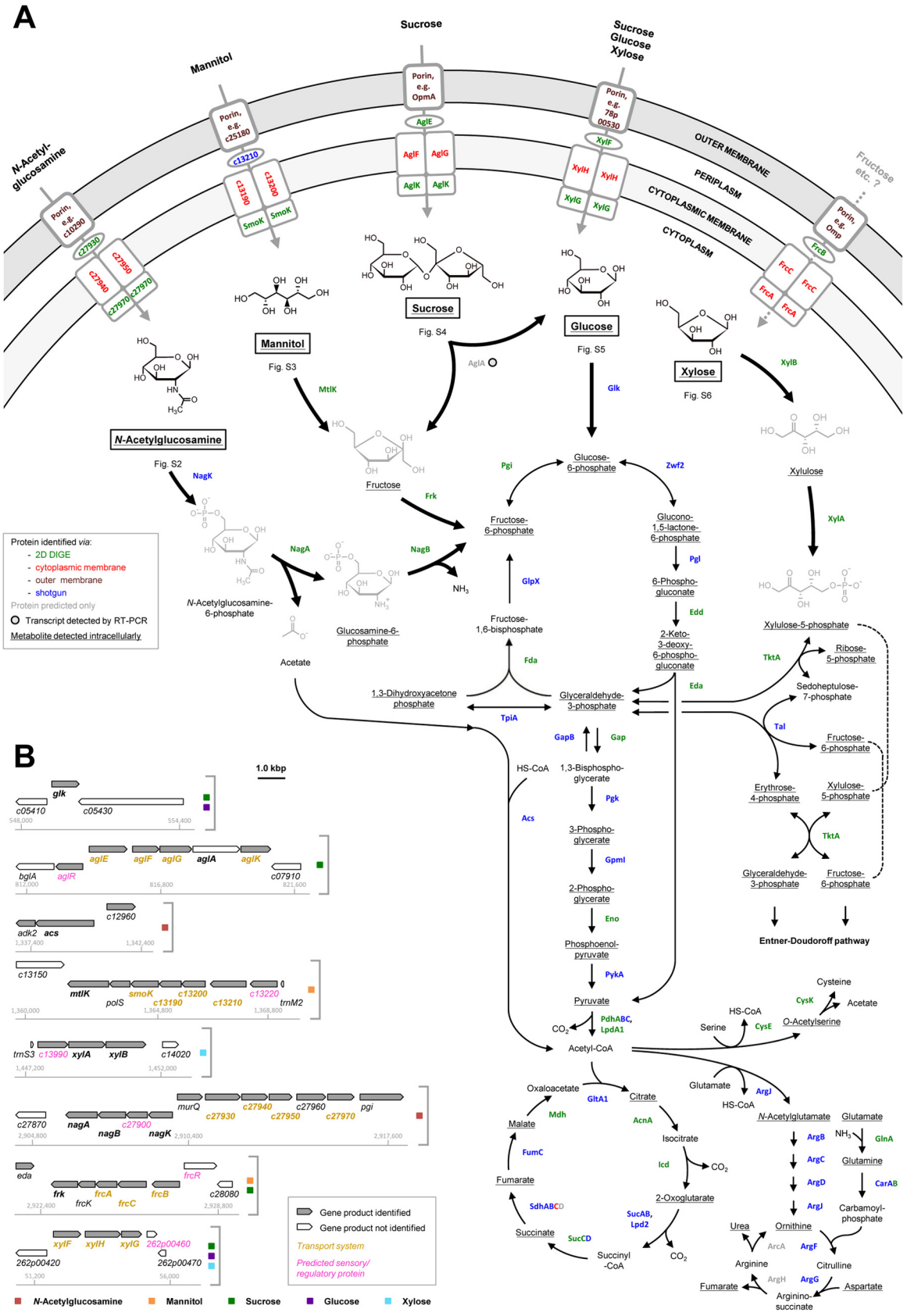

FIG 1 (A) Reconstruction of transport and degradation pathways for five selected carbohydrates in *P. inhibens* DSM 17395. The names, predicted functions, and proteomic data of the proteins indicated are summarized in Fig. 3. The metabolites detected are detailed in Fig. 4. Additional information for each of the five carbohydrates is provided in the supplemental material. (B) Genomic locations and contexts of genes encoding the transport systems and degradation enzymes. Genes whose products appear in panel A are shown in boldface. Additional information on predicted regulatory proteins is provided in Table S6 in the supplemental material.

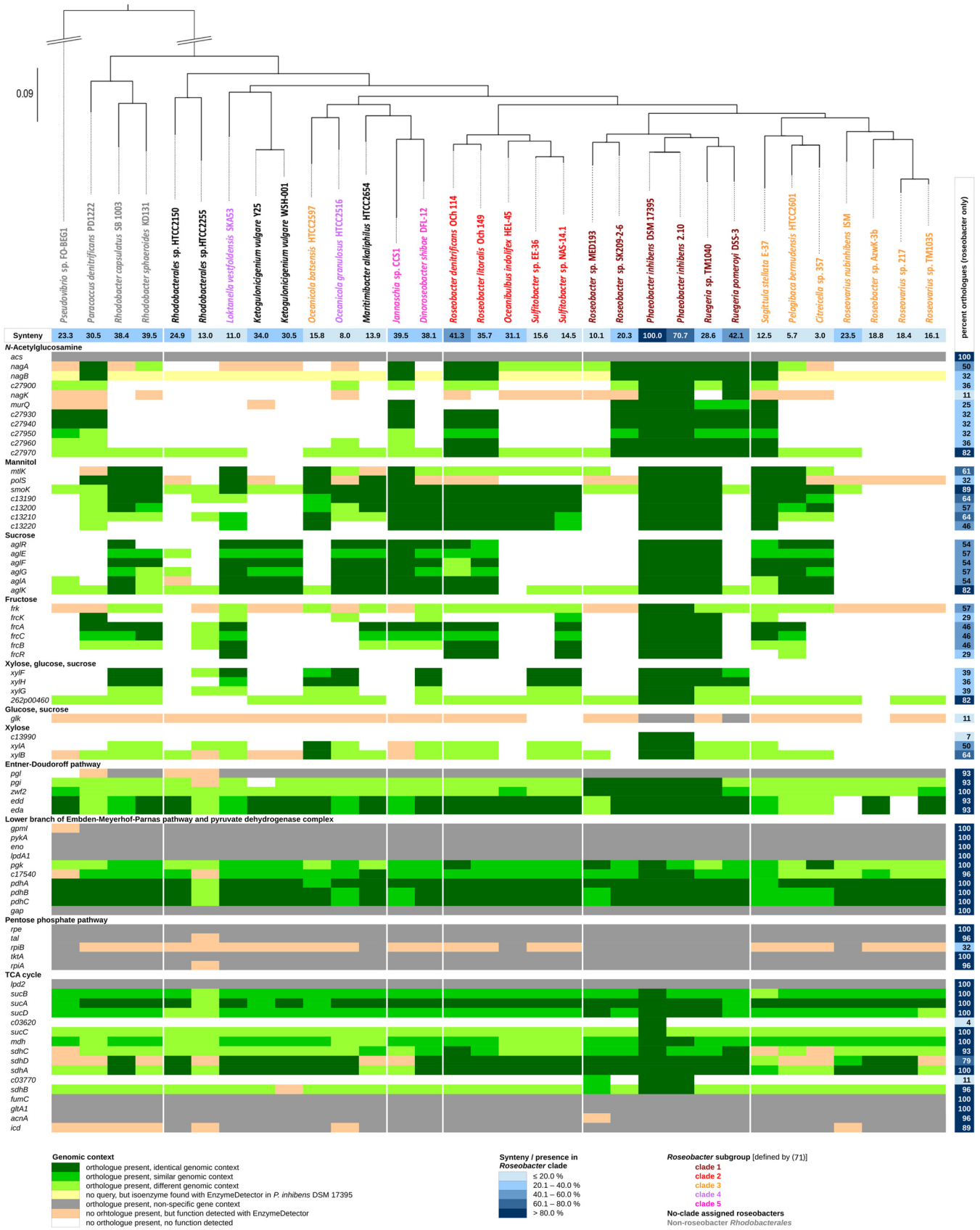
0.09
Pseudovibrio sp. FO-BEG1
Paracoccus denitrificans PD1222
Rhodobacter capsulatus SB 1003
Rhodobacter sphaeroides KD131
Rhodobacterales sp. HTCC2150
Rhodobacterales sp. HTCC2255
Loktanella vestfoldensis SKA53
Ketogulonicigenium vulgare Y25
Ketogulonicigenium vulgare WSH-001
Oceanicola batsensis HTCC2597
Oceanicola granulosus HTCC2516
Maritimibacter alkaliphilus HTCC2654
Jannaschia sp. CCS1
Dinoroseobacter shibae DFL-12
Roseobacter denitrificans OCh 114
Roseobacter litoralis Och 149
Oceanibulbus indolifex HEL-45
Sulfitobacter sp. EE-36
Sulfitobacter sp. NAS-14.1
Roseobacter sp. MED193
Roseobacter sp. SK209-2-6
Phaeobacter inhibens DSM 17395
Phaeobacter inhibens 2.10
Ruegeria sp. TM1040
Ruegeria pomeroyi DSS-3
Sagittula stellata E-37
Pelagibaca bermudensis HTCC2601
Citreicella sp. 357
Roseovarius nubinhibens ISM
Roseobacter sp. AzwK-3b
Roseovarius sp. 217
Roseovarius sp. TM1035
Synteny
23.3 30.5 38.4 39.5 24.9 13.0 11.0 34.0 30.5 15.8 8.0 13.9 39.5 38.1 41.3 35.7 31.1 15.6 14.5 10.1 20.3 100.0 70.7 28.6 42.1 12.5 5.7 3.0 23.5 18.8 18.4 16.1
percent orthologues (roseobacter only)
N-Acetylglucosamine
acs 100
nagA 50
nagB 32
c27900 36
nagK 11
murQ 25
c27930 32
c27940 32
c27950 32
c27960 36
c27970 82
Mannitol
mtlK 61
polS 32
smoK 89
c13190 64
c13200 57
c13210 64
c13220 46
Sucrose
aglR 54
aglE 57
aglF 54
aglG 57
aglA 54
aglK 82
Fructose
frk 57
frcK 29
frcA 46
frcC 46
frcB 46
frcR 29
Xylose, glucose, sucrose
xylF 39
xylH 36
xylG 39
262p00460 82
Glucose, sucrose
glk 11
Xylose
c13990 7
xylA 50
xylB 64
Entner-Doudoroff pathway
pgl 93
pgi 93
zwf2 100
edd 93
eda 93
Lower branch of Embden-Meyerhof-Parnas pathway and pyruvate dehydrogenase complex
gpmI 100
pykA 100
eno 100
lpdA1 100
pgk 100
c17540 96
pdhA 100
pdhB 100
pdhC 100
gap 100
Pentose phosphate pathway
rpe 100
tal 96
rpiB 32
tktA 100
rpiA 96
TCA cycle
lpd2 100
sucB 100
sucA 100
sucD 100
c03620 4
sucC 100
mdh 100
sdhC 93
sdhD 79
sdhA 100
c03770 11
sdhB 96
fumC 100
gltA1 100
acnA 96
icd 89
Genomic context
orthologue present, identical genomic context
orthologue present, similar genomic context
orthologue present, different genomic context
no query, but isoenzyme found with EnzymeDetector in P. inhibens DSM 17395
orthologue present, non-specific gene context
no orhtologue present, but function detected with EnzymeDetector
no orthologue present, no function detected
Synteny / presence in Roseobacter clade
≤ 20.0 %
20.1 – 40.0 %
40.1 – 60.0 %
60.1 – 80.0 %
> 80.0 %
Roseobacter subgroup [defined by (71)]
clade 1
clade 2
clade 3
clade 4
clade 5
No-clade assigned roseobacters
Non-roseobacter Rhodobacterales

rylated forms, both are important components of the cell wall polymer murein.

(ii) *N*-Acetylglucosamine and anabolism. In the absence of external *N*-acetylglucosamine, the murein building block UDP-*N*-acetylglucosamine has to be synthesized from fructose-6-phosphate by glucosamine-fructose-6-phosphate aminotransferase (GlmS), phosphoglucosamine mutase (GlmM), and the bifunctional enzyme GlmU, consisting of fused *N*-acetylglucosamine-1-phosphate uridyltransferase and glucosamine-1-phosphate acetyltransferase. As expected, these three enzymes were formed under all substrate conditions investigated except in *N*-acetylglucosamine-grown cells (see Table S4 in the supplemental material). Thus, *P. inhibens* DSM 17395 employs two different enzymes for the interconversion of glucosamine-6-phosphate and fructose-6-phosphate, i.e., GlmS for anabolic and NagB for catabolic purposes.

Degradation of *N*-acetylglucosamine yields acetyl-CoA via the catabolic pathway described above and via the lower part of the Embden-Meyerhof-Parnas (EMP) pathway. Acetyl-CoA can be used for the biosynthesis of, e.g., cysteine and arginine. The formation of cysteine involves acetyltransferase (CysE) and cysteine synthase (CysK) and proceeds via *O*-acetylserine. This intermediate possibly acts as a temporary acetyl sink and was more abundant in most carbohydrate-grown cells than in succinate-grown cells (Fig. 4). The first step of arginine biosynthesis is the ArgJ-catalyzed formation of *N*-acetylglutamate (specifically 6.8-fold more abundant in *N*-acetylglucosamine-grown cells than in succinate-grown cells) (Fig. 4). Except for the last enzyme (ArgH) of the biosynthetic sequence, all protein constituents (54) were identified (see Table S4 in the supplemental material). Proteins ArgFGH are also involved in the urea cycle employed by *P. inhibens* DSM 17395 to dispose of excess nitrogen as urea (24). Only slightly higher urea concentrations were detected in cells grown with the only nitrogen-containing substrate, *N*-acetylglucosamine, than in cells grown with the other four carbohydrates (Fig. 4). However, the possibility that the urea detected might also derive from cellular arginine decomposing during metabolic analysis should be considered.

(iii) Mannitol. *P. inhibens* DSM 17395 imports mannitol presumably via a specifically formed ABC transporter, c13180 to c13210 (Fig. 1A and 3), here reannotated as a mannitol ABC transporter (see Table S3 in the supplemental material). In addition, a second ABC transporter, c28030 to c28060, was detected in mannitol- and sucrose-grown cells. The genes encoding this transporter colocalize with the *frk* gene, encoding fructokinase (Fig. 1B). Thus, one may speculate that the formation of this transporter is activated by fructose, which is formed during the degradation of mannitol and sucrose. BLAST analyses supported reannotation as a fructose ABC transporter (FrcBCAK), as known from *Sinorhizobium meliloti* (55).

Mannitol is probably converted to fructose by the 2.5-fold-upregulated (in mannitol-grown cells compared to succinate-grown cells) NADH-dependent mannitol 2-dehydrogenase (MtlK; EC 1.1.1.67) (see Fig. S3 in the supplemental material), as known from the related enzyme in *Rhodobacter sphaeroides* Si4 (56). Mannitol and fructose were detected in the intracellular metabolome. Fructose is then phosphorylated by fructokinase (Frk; EC 2.7.1.4), yielding fructose-6-phosphate.

The *mtlK* gene is located next to genes encoding the mannitol ABC transporter c13180 to c13210 (Fig. 1B), separated merely by *polS* (encoding sorbitol dehydrogenase), as in *R. sphaeroides* Si4 (57). Thus, the ABC transporter might also be active with other polyols, e.g., sorbitol. Sorbitol dehydrogenase (PolS) was identified exclusively by shotgun analysis of mannitol-grown cells, suggesting that the complete gene cluster is transcribed. Notably, *P. inhibens* DSM 17395 can also use sorbitol as a growth substrate (see Table S1 in the supplemental material).

(iv) Sucrose. Differential proteomic data indicated sucrose uptake by the α-glucoside transport system (AglEFGK), as known from *S. meliloti* (58). The periplasmic binding protein (AglE) and the ATP-binding subunit (AglK) displayed the highest increases in abundance in sucrose-grown cells of *P. inhibens* DSM 17395 (Fig. 1A and 3). In addition to AglEFGK, two other ABC transporters are present in sucrose-grown cells: FrcBCAK (fructose) and XylFGH (xylose, fructose, and sucrose). Possibly, the formation of these two systems is coinduced by the sucrose degradation products fructose and glucose.

On the chromosome of *P. inhibens* DSM 17395, a predicted α-glucosidase (AglA) is encoded together with the genes of the sucrose transporter AglEFGK in an operon-like structure. Such an operon has been described previously for *S. meliloti* (58). Thus, one may assume that *P. inhibens* DSM 17395 also degrades sucrose to glucose and fructose by use of the α-glucosidase. While the AglA protein could not be identified in sucrose-grown cells, the *aglA* transcript was detected in sucrose-grown cells as well as in succinate-grown cells, indicating constitutive expression (see Fig. S4D in the supplemental material). The reaction products glucose and fructose were identified (Fig. 4) and could be further metabolized via phosphorylation by identified fructokinase (Frk) and glucokinase (Glk), respectively.

Notably, sucrose-grown cells contain a hypothetical protein, c11850 (92.1-fold upregulated in sucrose-grown cells compared to succinate-grown cells). It shows similarities to phage shock protein (PspA), which is generally associated with stress (59, 60). Growth with sucrose could result in a kind of growth-associated stress, since *P. inhibens* DSM 17395 displays the lowest μ_{max} (0.02 h^{-1}) with this substrate.

(v) Glucose. Glucose is presumably taken up by the ABC transporter XylFGH (Fig. 1A and 3). Accordingly, the periplasmic binding protein (XylF) was previously found to be more abundant in cells grown with glucose than in cells grown in complex Marine Broth (24).

For degradation, glucose is initially phosphorylated by glucokinase (Glk; EC 2.7.1.2; identified by shotgun analysis) to glucose-6-phosphate (see Fig. S5 in the supplemental material). Further degradation proceeds via the ED pathway. Glucose and

FIG 2 Genome comparison of *Roseobacter* clade members and non-*Roseobacter Rhodobacterales*. Shown are genes of *P. inhibens* DSM 17395 related to the carbohydrate transporters and degradation pathways investigated (the names and functional assignments are those shown in Fig. 1 and 3), as well as to central metabolism, with their respective orthologs in the other species. Where applicable, the genomic contexts of the genes were investigated, leading to categorization, with *P. inhibens* DSM 17395 set as a reference. Table S7 in the supplemental material lists the *P. inhibens* DSM 17395 genes analyzed, together with their locus tags, EC numbers, and corresponding enzyme names. The synteny and phylogenetic tree are as previously published (26).

Acc. No. (PGA1_)	Name	Predicted function[a]	Fold change[b] in abundance (2D DIGE)					Mascot score (gel-free analysis)														
								NAG			MTL			SUCR			GLC			XYL			Succ		
			NAG	MTL	SUCR	GLC	XYL	S	CM	OM	S	CM	OM	S	CM	OM	S	CM	OM	S	CM	OM	S	CM	OM
TRANSPORT																									
Outer membrane proteins																									
c33380	OpmA	Porin	-1.0	-3.9	-2.7	-5.7	-4.8	326	577	1158	452	808	1189	390	678	1147	315	697	1067	447	621	1019	478	495	1019
c06130		Outer membrane protein OmpA-like protein								240		115	63		94			111			183	66		34	126
c14280	Omp	Outer membrane protein						562	704	1036	400	678	1409	539	465	743	302	796	1236	287	385	1379	878	271	1379
c10290		Outer membrane protein								72															
78p00530		Putative outer membrane protein											76			33			84			53			106
c25180		Outer membrane protein-like protein								67			131						38						
78p00400		TonB dependent receptor								173			313						326			56			
N-Acetylglucosamine																									
c27930		*N*-Acetylglucosamine ABC transporter, periplasmic sugar-binding protein[d]	26.1	-1.5	-4.1	-3.4	-3.6	1267						286						129			310		
c27940		*N*-Acetylglucosamine ABC transporter, permease[d]							90																
c27950		*N*-Acetylglucosamine ABC transporter, permease[d]							172			85									28				
c27970		*N*-Acetylglucosamine ABC transporter, ATP-binding protein[d]	2.4	-6.4	-5.9	-5.7	-11.7	841	486			47													
Mannitol																									
c13180	SmoK[d]	Mannitol ABC transporter, ATP-binding transport protein[d]	-1.3	4.9	-1.1	-1.1	-1.2	105			991	218											140		
c13190		Mannitol ABC transporter, permease[d]										311													
c13200		Mannitol ABC transporter, permease[d]										138													
c13210		Mannitol ABC transporter, periplasmic sugar-binding protein[d]									933														
Sucrose																									
c07860	AglE	Alpha-glucoside ABC transporter, periplasmic sugar-binding protein[d]	1.3	-2.7	29.1	-1.0	-1.6							622											
c07870	AglF	Alpha-glucoside ABC transporter, permease[d]													35										
c07880	AglG	Alpha-glucoside ABC transporter, permease[d]													247										
c07900	AglK	Alpha-glucoside ABC transporter, ATP-binding transport protein[d]	1.3	1.7	6.8	1.7	1.7							372	80										
Xylose, glucose, sucrose																									
262p00430	XylF[c]	Xylose ABC transporter, periplasmic sugar-binding protein[c]	1.8	-3.8	3.2	7.3	11.8	349						569			773			863			114		
262p00440	XylH	Xylose ABC transporter, permease[b]																220			203				
262p00450	XylG[c,d]	Xylose ABC transporter, ATP-binding protein[c,d]	-1.5	-3.0	4.9	20.8	21.6							271			634	117		687	31				
Fructose																									
c28030	FrcK[d]	Fructose ABC transporter, kinase[d]										127			184										
c28040	FrcA[d]	Fructose ABC transporter, ATP-binding protein[d]									118	78			110	48									
c28050	FrcC[d]	Fructose ABC transporter, permease[d]										68			127			30			69				
c28060	FrcB[d]	Fructose ABC transporter, periplasmatic sugar-binding protein[d]	1.8	2.3	6.8	1.3	1.2	324			609			670									78		
Succinate																									
c20660	DctM6[d]	TRAP transporter, transmembrane subunit[d]																			35			76	
c20670	DctQ6[d]	TRAP transporter, transmembrane subunit[d]																86			55			145	
c20680	DctP6[c,d]	TRAP transporter, periplasmic solute-binding protein[c,d]	-13.8	-40.9	-32.1	-32.4	-21.1	247			127			580			152			134			805		
CARBOHYDRATE METABOLISM																									
N-Acetylglucosamine																									
c27910	NagK[d]	*N*-Acetylglucosamine kinase[d]						414																	
c27880	NagA	*N*-Acetylglucosamine-6-phosphate deacetylase	3.8	1.4	-1.0	1.4	-1.3	264																	
c27890	NagB[d]	Glucosamine-6-phosphate deaminase[d]	15.6	-1.1	-1.8	-2.1	-2.0	858	322																
c12950	Acs	Acetyl-coenzyme A synthetase						607	58		464			188			400			243	33		322		
Mannitol																									
c13160	MtlK	Mannitol 2-dehydrogenase	1.3	2.5	1.5	1.6	1.7				492	250													
c28020	Frk	Fructokinase	1.6	1.5	2.2	-1.1	1.1																		
Sucrose																									
c28020	Frk	Fructokinase	1.6	1.5	2.2	-1.1	1.1																		
c05420	Glk	Glucokinase						246			296			194	57		341			286			97		
Glucose																									
c05420	Glk	Glucokinase						246			296			194	57		341			286			97		
Xylose																									
c14000	XylA[c]	Xylose isomerase[c]	1.0	-1.2	1.0	-1.2	5.0											112		1276					
c14010	XylB	Xylulose kinase	-1.4	1.4	1.3	1.9	17.2													649					

[a] For original annotation refer to Table S2 in the supplemental material.
[b] As compared to succinate-adapted cells of *P. inhibens* DSM 17395.
[c] Identified from multiple spots on a single 2DE gel.
[d] For annotation refinement or full enzyme names see Table S3 in the supplemental material.

Fold change: n.d. | < -30.0 | < -10.0 | < -5.0 | < -1.5 | > - 1.5 | > 1.5 | > 5.0 | > 10.0 | > 35.0

Mascot score: n.d. | > 25 | > 200 | > 500 | > 1000

FIG 3 Selected proteins of *P. inhibens* DSM 17395 identified from 2DE gels (2D DIGE), by shotgun analysis (S), and from fractions enriched in cytoplasmic membrane protein (CM) or outer membrane protein (OM) and resolved by SDS-PAGE (see also Fig. S8 in the supplemental material). Proteins involved in carbohydrate transport and degradation pathways or in central metabolism are shown. Abbreviations of substrates: NAG, *N*-acetylglucosamine; MTL, mannitol; SUCR, sucrose; GLC, glucose; XYL, xylose; Succ, succinate.

glucose-6-phosphate were detected in the intracellular metabolome. The *glk* gene has a solitary localization on the chromosome of *P. inhibens* DSM 17395 (Fig. 1B). The presence of its product, Glk, under all substrate conditions tested could point to constitutive expression (Fig. 3).

(vi) Xylose. The uptake of xylose is assumed to involve the ABC transporter XylFGH, since the two soluble subunits (XylFG) displayed the greatest abundance increases in xylose-grown cells compared to succinate-grown cells (11.8-fold and 21.6-fold, respectively [Fig. 3]). Thus, the solute range of the XylFGH system

Metabolites[a]	Fold change[b]				
	NAG	MTL	SUCR	GLC	XYL
CARBOHYDRATE METABOLISM					
N-Acetylglucosamine	12.02	1.33	1.69	2.65	1.36
Glucose/ Glucosamine/ Sorbitol-6-phosphate	0.03	0.12	0.66	47.27	0.33
Glucosamine	0.49		0.12		0.12
Mannitol	0.76	19.86	1.02	0.47	0.43
Fructose	0.73	8.27	17.29	2.21	1.05
Sucrose			#		
Glucose	1.59	2.00	0.78	1.04	0.86
Xylose			#		##
Xylulose	0.81	0.76	0.52	0.87	0.87
CENTRAL METABOLISM					
Entner-Doudoroff pathway					
Fructose-6-phosphate	0.07	0.02	4.28	4.30	0.44
Glucose/ Galactose/ Mannose-6-phosphate	0.03	0.04	0.16	0.30	0.14
Glucono-1,5-lactone *	4.70	8.99	9.83	22.36	4.99
Galactonate/ Gluconate *	11.38	4.62	8.06	25.95	6.58
6-Phosphogluconate	0.24	0.96	5.05	15.77	0.17
2-Keto-3-deoxy-D-gluconate (KDG) *	30.50	4.66	1.87	3.18	2.05
Glyceraldehyde *	1.05	0.75	0.50	0.64	0.76
Lower branch of Embden-Meyerhof Parnas pathway					
Dihydroxyacetonephosphate	1.68	0.31	0.39	0.63	0.60
1,3-Dihydroxyacetone *	0.77	0.95	1.00	1.12	0.98
3-Phosphoglycerate	3.77	1.58	1.66	8.75	2.60
2-Phosphoglycerate	1.64	0.42	0.80	2.70	
Phosphoenolpyruvate	1.95	1.77	1.27	4.43	1.84
Pyruvate	7.71	3.62	3.11	3.84	5.35
Pentose phosphate pathway					
Erythrose-4-phosphate	3.74	2.75	5.45	0.48	0.99
Ribose	1.02	2.30	0.81	0.89	2.45
Xylulose-/ Ribulose-5-phosphate	0.09		0.05	0.17	1.00
TCA cycle					
Citrate	4.00	1.28	0.89	5.06	4.39
2-Oxoglutarate	1.90	0.73	0.60	1.10	1.31
Succinate	0.60	0.30	0.07	0.13	0.24
Fumarate	2.11	0.71	0.35	0.37	0.52
Malate	3.45	0.48	0.28	0.34	0.40
AMINO ACID DERIVATIVES					
N-Acetylglutamate	6.77	0.78		0.87	1.08
O-Acetylserine	18.63	11.83	0.91	3.08	11.50
Ornithine	1.46	0.41	0.22	0.38	1.04
ORGANIC ACIDS					
Erythronate	8.23	2.70	1.61	2.90	1.91
Tartrate	0.68	1.59	10.82	168.67	3.06
Threonate	2.59	4.20	29.65	13.08	2.64
Urea	0.98	0.80	0.26	0.69	0.27

n.d.	< 0.10	< 0.34	< 0.66	0.67 - 1.50	> 1.50	> 2.50	> 5.00	> 10.00

[a], Information on all 116 identified intracelluar metabolites is provided in Table S5 in the supplemental material.

[b], Fold change in metabolite abundance as compared to cells grown with succinate.

#, Compound not detected in reference.

##, Compound not detected in reference; but intense peak in corresponding cultivation condition.

*, Probably dephosphorylated during extraction.

FIG 4 Fold changes in abundances of selected intracellular metabolites of *P. inhibens* DSM 17395. For all intracellular metabolites of *P. inhibens* DSM 17395 identified in this study, see Table S5 in the supplemental material. Abbreviations of substrates: NAG, *N*-acetylglucosamine; MTL, mannitol; SUCR, sucrose; GLC, glucose; XYL, xylose.

in *P. inhibens* DSM 17395 may include xylose as well as glucose and sucrose (see above).

The degradation of xylose is initiated via isomerization to xylulose. As is known from enterobacteria (61, 62) and the marine bacterium *Rhodopirellula baltica* (63), this isomerization is performed by xylose isomerase (XylA), which was 5.0-fold more abundant in xylose-grown cells than in succinate-grown cells (see Fig. S6 in the supplemental material). Xylulose is then phosphorylated to xylulose-5-phosphate by xylulose kinase (XylB; 17.2-fold more abundant in xylose-grown cells than in succinate-grown cells). Both metabolites were detected in the intracellular fraction. Following the entry of xylulose-5-phosphate into the pentose phosphate pathway, fructose-6-phosphate is formed, which is further metabolized via the ED pathway.

In contrast to the pattern in *E. coli* K-12 (62), the genes for xylose degradation and transport do not colocalize in *P. inhibens* DSM 17395. Rather, *xylAB* form an operon-like structure on the chromosome, whereas *xylFGH* do so on the 262-kbp plasmid (Fig. 1B).

Regulation. (i) Transporters for carbohydrates and succinate. Differential subcellular proteomics combined with genomic analysis in the present study revealed that *P. inhibens* DSM 17395 does not employ phosphotransferase systems (PTS) to import carbohydrates, as do *E. coli* and other bacteria (64). Rather, *P. inhibens* DSM 17395 uses ABC transporters. While these are less energy efficient than PTS, they are highly efficient at very low external substrate concentrations (up to a 10^4-fold concentration difference) (65), such as those encountered in the mostly oligotrophic environments of roseobacters. The substrate specificity of ABC transporter formation could be classified into three levels of stringency. The ABC transporters for *N*-acetylglucosamine, mannitol, and sucrose were formed with high substrate specificity, agreeing with the tight genomic association of their coding genes with the genes for the respective catabolic enzymes and proposed regulators (Fig. 1B; see also Table S6 in the supplemental material). In contrast, the XylFHG transporter, which is the only ABC transporter separately encoded on the 262-kbp plasmid, was identified in xylose-, glucose-, and sucrose-grown cells. Despite the colocalization of its genes with that for fructokinase (Frk) and the gene encoding the sensory/regulatory protein FrcR, the fructose transporter (FrcBCAK) was identified in mannitol- and sucrose-grown cells. Possibly, fructose as an intermediate of mannitol and sucrose degradation could serve as an inducer, as shown previously for *S. meliloti* (55).

In contrast to the carbohydrates, succinate is assumed to be taken up by *P. inhibens* DSM 17395 via the tripartite ATP-independent periplasmic (TRAP) transporter (DctM6P6Q6 [Fig. 3]). This system consists of two transmembrane proteins (DctMQ) and a periplasmic solute-binding protein (DctP) and was demonstrated in *Rhodobacter capsulatus* as a high-affinity transport system for succinate and other C_4 dicarboxylates (66). Since TRAP transporters are ATP independent, the transport of succinate into the cells is less energy-consuming than the uptake of the carbohydrates studied.

(ii) Peripheral degradation pathways. Most enzymes involved in channeling individual carbohydrates into the central metabolism are formed with high substrate specificity (Fig. 3). Six predicted regulatory/sensory proteins could serve as possible mediators of the underlying tight control of gene expression, since they are encoded in juxtaposition with the "catabolic" genes (Fig. 1B;

see also Table S6 in the supplemental material). Four of these proteins were detected in the present study, and three of these are related to the LacI family of transcriptional regulators. The first, c07850 (reannotated as AglR), is more abundant in sucrose-grown cells than in succinate-grown cells and might regulate the expression of *aglEFGK* and *aglA*, as proposed previously for *S. meliloti* (58). The second, c13220, was specifically identified in mannitol-grown cells and probably controls the transcription of *mtlK* and the genes for the mannitol ABC transporter. The third, c13990, was specifically detected in xylose-grown cells and possibly regulates *xylAB* expression. The fourth probable regulatory protein identified is the GntR family-type transcriptional regulator c27900, which was identified exclusively in *N*-acetylglucosamine-grown cells and might control the expression of genes for the uptake and degradation of this amino sugar.

(iii) Central metabolism. Following the formation of fructose-6-phosphate or glucose-6-phosphate, further metabolism proceeds via the ED pathway, connecting into the lower branch of the EMP pathway (see Fig. S9 in the supplemental material) (22, 23). Accordingly, the protein constituents of both pathways identified are abundant in cells adapted to any of the five carbohydrates tested, compared to succinate-adapted cells (see Table S4 in the supplemental material). This general profile was also observed with the respective metabolites identified (Fig. 4).

In succinate-utilizing cells, carbohydrates have to be generated via gluconeogenesis (see Fig. S12 in the supplemental material), involving pyruvate carboxylase (Pyc), phosphoenolpyruvate carboxykinase (PckA), glyceraldehyde-3-phosphate dehydrogenase 2 (GapB), and fructose-bisphosphate aldolase class 1 (Fda). As expected, these enzymes are mostly more abundant in succinate-adapted than in carbohydrate-adapted cells.

In contrast, proteins of the pentose phosphate pathway (see Fig. S10 in the supplemental material), pyruvate dehydrogenase complex, and TCA cycle (see Fig. S11 in the supplemental material) display mainly unchanged abundances across all six substrate conditions analyzed. This was also observed previously, when *P. inhibens* DSM 17395 was grown with nine different amino acids (26) and was analyzed for growth phase response (22). Notably, *P. inhibens* DSM 17395 does not possess a phosphogluconate dehydrogenase generating ribulose-5-phosphate from 6-phosphogluconate, indicating that the oxidative branch of the pentose phosphate pathway is not active.

Formation of C_4 carboxylates. Notably, *P. inhibens* DSM 17395 produces large amounts of threonate, erythronate, and tartrate during growth with carbohydrates (Fig. 4). It is not clear at present how these C_4 carboxylates are formed and why. One may speculate that they are formed from erythrose-4-phosphate, an intermediate of the pentose phosphate pathway, which could be oxidized to 4-phospho-erythronate by an erythrose-4-phosphate dehydrogenase-like enzyme. In *E. coli* K-12 (67), this enzyme is involved in pyridoxine and pyridoxal-5′-phosphate biosynthesis. Notably, glycerol-aldehyde-3-phosphate dehydrogenase (Gap) from *P. inhibens* DSM 17395 shows high similarity to erythrose-4-phosphate dehydrogenase of *E. coli* K-12 (E value, $1e^{-108}$). Thus, abundantly formed Gap (see Table S4 in the supplemental material) may transform erythrose-4-phosphate in a side reaction. Dephosphorylation of the reaction product 4-phospho-erythronate would yield erythronate and its isomer threonate. In plants it was observed that threonate could be oxidized to tartrate (68). However, except for the possible involvement of Gap, no enzymes for the formation of erythronate, threonate, and tartrate could be delineated from the genome or the proteomic data.

Entner-Doudoroff pathway. This study demonstrated that *P. inhibens* DSM 17395 uses the ED pathway (see Fig. S9 in the supplemental material) not only for the degradation of glucose (22, 23) but also for other carbohydrates. With the ED pathway, *P. inhibens* DSM 17395 gains, per mol of glucose-6-phosphate, 1 mol each of ATP, NADH, and NADPH instead of 2 mol of ATP and 2 mol of NADH, which are obtained if the EMP pathway is employed. To put it simply, 1 mol NADPH is formed instead of 1 mol each of ATP and NADH. NADPH is important for anabolic reactions, such as amino acid and fatty acid biosynthesis. It has been suggested that in a metabolic model of *E. coli*, most of the NADPH required is formed by the oxidative pentose phosphate pathway (69). Because the latter is not operative in *P. inhibens* DSM 17395, the ED pathway is supposed to take over its role in NADPH production. The advantage of using the ED pathway is that NADPH is generated directly without the need for transhydrogenases. In *P. inhibens* DSM 17395, the NAD(P) transhydrogenase (PntAB) is located in the cytoplasmic membrane (see Table S4 in the supplemental material), and the subunits have 5 and 10 transmembrane helices, respectively. Membrane-localized transhydrogenases use the proton electrochemical gradient to convert NADH and $NADP^+$ to NAD^+ and NADPH and thereby use energy indirectly (70). Considering the energy expenditure of transhydrogenases, the balance for the ED pathway approximates that of the EMP pathway.

Comparative genomics. A total of 74 genes involved in the reconstructed carbohydrate catabolic network (Fig. 1 and 3) and central metabolism (see Table S4 in the supplemental material) were analyzed for their dissemination across *Rhodobacterales* (Fig. 2) and other heterotrophic members of the marine bacterioplankton (see Fig. S7 in the supplemental material). The query genes of *P. inhibens* DSM 17395 are compiled in Table S7 in the supplemental material, and those of the other *Rhodobacterales* selected for the comparative analysis have been reported recently (26).

Homologous enzymes of the central metabolism are widespread (average dissemination, 93% of genomes) across roseobacters. For example, three genes of the pyruvate dehydrogenase complex (*pdhABC*) are present in all genomes investigated and are mostly arranged in a genomic context identical to that in *P. inhibens* DSM 17395. The two key enzymes of the ED pathway (Edd and Eda) are encoded in 93% of the roseobacter genomes investigated (except for *Roseovarius nubinhibens* ISM and *Roseovarius* sp. strain 217, both from clade 2), corroborating our earlier observation on the general role of the ED pathway among roseobacters (22, 23).

In comparison to the central metabolism, homologous genes for carbohydrate transport, peripheral degradation, and regulation were less widespread among the roseobacter genomes analyzed (present in 48%). In particular, *Roseobacter* clade 3 members possess only a few homologs, while in the closely related but geographically distant strain *P. inhibens* 2.10, all genes not only are present but occur in the identical genomic context. In the case of *N*-acetylglucosamine, genes for the complete transporter are present in 11 genomes, mainly from clade 1, but also from clades 2, 3, and 5 and from non-*Roseobacter Rhodobacterales*. The reannotated *N*-acetylglucosamine kinase (*nagK*) could be found only in *P. inhibens* 2.10 and *Ruegeria pomeroyi* DSS-3, two other clade 1 members. However, in 41% of the genomes investigated, a non-

homologous enzyme replaces *P. inhibens* NagK. Genes involved in the uptake and initial conversion of sucrose and mannitol, as well as in their respective regulation, are present in more than half of the roseobacter genomes investigated. The only exception is the existence of sorbitol dehydrogenase, the coding gene of which (*polS*) is present in only 32% of the roseobacter genomes investigated. The genes coding for the fructose ABC transporter (*frcABC*) are confined to 46% of the roseobacter genomes, whereas the corresponding regulator (*frcR*) and a kinase (*frcK*) are present in only 29% of the genomes. The dissemination of the *glk* gene, encoding glucokinase, is restricted to *P. inhibens* 2.10 and *Ruegeria pomeroyi* DSS-3. Although the xylose degradation enzymes XylAB are encoded in about half of the genomes investigated, the corresponding regulator c13990 is confined to the two *P. inhibens* species analyzed.

Other heterotrophic members of the marine bacterioplankton, such as "*Candidatus* Pelagibacter" spp., *Cytophaga* spp., *Flavobacterium* spp., *Gramella* spp., or *Polaribacter* spp., possess considerably fewer homologs of the query genes: 28% of the genes involved in central metabolism and only 5% of the genes involved in carbohydrate transport, peripheral degradation, and regulation (see Fig. S7 in the supplemental material). Most of the functionalities unaccounted for in the central metabolism (except for the ED pathway) could be assigned in these bacteria based on the detection of nonorthologous genes by EnzymeDetector. Notably, however, such nonorthologous functions were mostly not found for the peripheral degradation reactions studied and the ED pathway in the selected non-*Roseobacter* heterotrophic bacteria (see Fig. S7 in the supplemental material). Taking our findings together, the *P. inhibens* DSM 17395 genes investigated here are present to various degrees in the different *Roseobacter* clades, as recently reported for genes of *P. inhibens* DSM 17395 involved in amino acid degradation (26). They could reflect an evolutionary shaping of roseobacter genomes directed at metabolic streamlining to optimize the habitat functioning and niche differentiation of this important group of marine bacteria.

Conclusion. This study allowed the reconstruction of transport systems and degradation pathways of five environmentally relevant carbohydrates in the model roseobacter *P. inhibens* DSM 17395. One of the most abundant carbohydrates in the world's oceans is the chitin monomer *N*-acetylglucosamine. Correspondingly, among the five carbohydrates tested, the fastest growth of *P. inhibens* DSM 17395 was observed with this compound. Based on the original genome annotation, only two proteins (NagK and Acs) were associated with *N*-acetylglucosamine degradation. By means of proteogenomics, this study revealed two additional catabolic enzymes, a predicted regulatory protein, and a complete ABC transport system, all of which were formed exclusively in the presence of *N*-acetylglucosamine. These proteins are not restricted to *P. inhibens* DSM 17395 but are also predicted for most of the members of *Roseobacter* clade 1 whose genomes have been sequenced.

It is noteworthy that highly substrate specific formation of metabolic modules (regulators, uptake system, and catabolic enzymes) was observed for all five carbohydrates investigated, indicating a fine-tuned regulatory network similar to that observed recently for the degradation of nine selected amino acids in *P. inhibens* DSM 17395 (26). Taking these results together, such metabolic adaptability could be advantageous for coping with the naturally fluctuating availability of carbohydrates and other organic substrates in marine systems.

Considering that roseobacters contribute significantly to marine carbohydrate catabolism, the multiple new functional assignments of the present study could be beneficial for the metabolic interpretation of the steadily increasing marine meta-omics data.

ACKNOWLEDGMENTS

We are grateful to R. Gahl-Janssen (Oldenburg, Germany) for growth tests with carbohydrates and to C. Hinrichs (Oldenburg, Germany) and D. Thies (Bremen, Germany) for experimental support with 2D DIGE and 2DE. We thank K. Trautwein (Oldenburg, Germany), S. Koßmehl (Oldenburg, Germany), and K. Schmidt-Hohagen (Braunschweig, Germany) for expert discussions. We are indebted to F. Widdel for general support of proteomic work in our group.

This study was supported by the Deutsche Forschungsgemeinschaft (SFB TRR 51).

REFERENCES

1. **Pakulski JD, Benner R.** 1994. Abundance and distribution of carbohydrates in the ocean. Limnol. Oceanogr. **39:**930–940. http://dx.doi.org/10.4319/lo.1994.39.4.0930.
2. **Yang C, Rodionov DA, Xiaoqing L, Laikova ON, Gelfand MS, Zagnitko OP, Romine MF, Obraztsova AY, Nealson KH, Osterman AL.** 2006. Comparative genomics and experimental characterization of *N*-acetylglucosamine utilization pathway of *Shewanella oneidensis*. J. Biol. Chem. **281:**29872–29885. http://dx.doi.org/10.1074/jbc.M605052200.
3. **Kirchman DL, White J.** 1999. Hydrolysis and mineralization of chitin in the Delaware estuary. Aquat. Microb. Ecol. **18:**187–196. http://dx.doi.org/10.3354/ame018187.
4. **Benner R, Kaiser K.** 2003. Abundance of amino sugars and peptidoglycan in marine particulate and dissolved organic matter. Limnol. Oceanogr. **48:**118–128. http://dx.doi.org/10.4319/lo.2003.48.1.0118.
5. **Rich JH, Ducklow HW, Kirchman DL.** 1996. Concentrations and uptake of neutral monosaccharides along 140°W in the equatorial Pacific: contribution of glucose to heterotrophic bacterial activity and the DOM flux. Limnol. Oceanogr. **41:**595–604. http://dx.doi.org/10.4319/lo.1996.41.4.0595.
6. **Skoog A, Benner R.** 1997. Aldoses in various size fractions of marine organic matter: implications for carbon cycling. Limnol. Oceanogr. **42:**1803–1813. http://dx.doi.org/10.4319/lo.1997.42.8.1803.
7. **Iwamoto K, Shiraiwa Y.** 2005. Salt-regulated mannitol metabolism in algae. Mar. Biotechnol. **7:**407–415. http://dx.doi.org/10.1007/s10126-005-0029-4.
8. **Reid SJ, Abratt VR.** 2005. Sucrose utilisation in bacteria: genetic organization and regulation. Appl. Microbiol. Biotechnol. **67:**312–321. http://dx.doi.org/10.1007/s00253-004-1885-y.
9. **Poretsky RS, Sun S, Mou X, Moran MA.** 2010. Transporter genes expressed by coastal bacterioplankton in response to dissolved organic carbon. Environ. Microbiol. **12:**616–627. http://dx.doi.org/10.1111/j.1462-2920.2009.02102.x.
10. **Alonso C, Pernthaler J.** 2006. *Roseobacter* and SAR11 dominate microbial glucose uptake in coastal North Sea waters. Environ. Microbiol. **8:**2022–2030. http://dx.doi.org/10.1111/j.1462-2920.2006.01082.x.
11. **Wagner-Döbler I, Biebl H.** 2006. Environmental biology of the marine *Roseobacter* lineage. Annu. Rev. Microbiol. **60:**255–280. http://dx.doi.org/10.1146/annurev.micro.60.080805.142115.
12. **Thole S, Kalhöfer D, Voget S, Berger M, Engelhardt T, Liesegang H, Wollherr A, Kjelleberg S, Daniel R, Simon M, Thomas T, Brinkhoff T.** 2012. *Phaeobacter gallaeciensis* genomes from globally opposite locations reveal high similarity of adaptation to surface life. ISME J. **6:**2229–2244. http://dx.doi.org/10.1038/ismej.2012.62.
13. **Buddruhs N, Pradella S, Göker M, Päuker O, Pukall R, Spröer C, Schumann P, Petersen J, Brinkhoff T.** 2013. Molecular and phenotypic analyses reveal the non-identity of the *Phaeobacter gallaeciensis* type strain deposits CIP 105210^T and DSM 17395. Int. J. Syst. Evol. Microbiol. **63:**4340–4349. http://dx.doi.org/10.1099/ijs.0.053900-0.
14. **Zhang D-C, Li H-R, Xin YH, Liu H-C, Chi Z-M, Zhou P-J, Yu Y.** 2008. *Phaeobacter arcticus* sp. nov., a psychrophilic bacterium isolated from the

Arctic. Int. J. Syst. Evol. Microbiol. **58:**1384–1387. http://dx.doi.org/10.1099/ijs.0.65708-0.
15. **Yoon J-H, Kang S-J, Lee S-Y, Oh T-K.** 2007. *Phaeobacter daeponensis* sp. nov., isolated from a tidal flat of the Yellow Sea in Korea. Int. J. Syst. Evol. Microbiol. **57:**856–861. http://dx.doi.org/10.1099/ijs.0.64779-0.
16. **Gaboyer F, Tindall BJ, Ciobanu M-C, Duthoit F, Le Romancer M, Alain K.** 2013. *Phaeobacter leonis* sp. nov., an alphaproteobacterium from Mediterranean Sea sediments. Int. J. Syst. Evol. Microbiol. **63:**3301–3306. http://dx.doi.org/10.1099/ijs.0.046128-0.
17. **Brinkhoff T, Bach G, Heidorn T, Liang L, Schlingloff A, Simon M.** 2004. Antibiotic production by a *Roseobacter* clade-affiliated species from the German Wadden Sea and its antagonistic effects on indigenous isolates. Appl. Environ. Microbiol. **70:**2560–2565. http://dx.doi.org/10.1128/AEM.70.4.2560-2565.2003.
18. **Vandecandelaere I, Segaert E, Mollica A, Faimali M, Vandamme P.** 2009. *Phaeobacter caeruleus* sp. nov., a blue-coloured, colony-forming bacterium isolated from a marine electroactive biofilm. Int. J. Syst. Evol. Microbiol. **59:**1209–1214. http://dx.doi.org/10.1099/ijs.0.002642-0.
19. **Ruiz-Ponte C, Cilia V, Lambert C, Nicolas JL.** 1998. *Roseobacter gallaeciensis* sp. nov., a new marine bacterium isolated from rearings and collectors of the scallop *Pecten maximus*. Int. J. Syst. Evol. Microbiol. **48:**537–542.
20. **Berger M, Neumann A, Schulz S, Simon M, Brinkhoff T.** 2011. Tropodithietic acid production in *Phaeobacter gallaeciensis* is regulated by *N*-acyl homoserine lactone-mediated quorum sensing. J. Bacteriol. **193:**6576–6585. http://dx.doi.org/10.1128/JB.05818-11.
21. **Martens T, Heidorn T, Pukall R, Simon M, Tindall BJ, Brinkhoff T.** 2006. Reclassification of *Roseobacter gallaeciensis* Ruiz-Ponte *et al.* 1998 as *Phaeobacter gallaeciensis* gen. nov., comb. nov., description of *Phaeobacter inhibens* sp. nov., reclassification of *Ruegeria algicola* (Lafay *et al.* 1995) Uchino *et al.* 1999 as *Marinovum algicola* gen. nov., comb. nov., and emended descriptions of the genera *Roseobacter*, *Ruegeria* and *Leisingera*. Int. J. Syst. Evol. Microbiol. **56:**1293–1304. http://dx.doi.org/10.1099/ijs.0.63724-0.
22. **Zech H, Thole S, Schreiber K, Kalhöfer D, Voget S, Brinkhoff T, Simon M, Schomburg D, Rabus R.** 2009. Growth phase-dependent global protein and metabolite profiles of *Phaeobacter gallaeciensis* strain DSM 17395, a member of the marine *Roseobacter*-clade. Proteomics **9:**3677–3697. http://dx.doi.org/10.1002/pmic.200900120.
23. **Fürch T, Preusse M, Tomasch J, Zech H, Wagner-Döbler I, Rabus R, Wittmann C.** 2009. Metabolic fluxes in the central carbon metabolism of *Dinoroseobacter shibae* and *Phaeobacter gallaeciensis*, two members of the marine *Roseobacter* clade. BMC Microbiol. **9:**209. http://dx.doi.org/10.1186/1471-2180-9-209.
24. **Zech H, Hensler M, Koßmehl S, Drüppel K, Wöhlbrand L, Trautwein K, Hulsch R, Maschmann U, Colby T, Schmidt J, Reinhardt R, Schmidt-Hohagen K, Schomburg D, Rabus R.** 2013. Adaptation of *Phaeobacter inhibens* DSM 17395 to growth with complex nutrients. Proteomics **13:**2851–2868. http://dx.doi.org/10.1002/pmic.201200513.
25. **Zech H, Hensler M, Koßmehl S, Drüppel K, Wöhlbrand L, Trautwein K, Colby T, Schmidt J, Reinhardt R, Schmidt-Hohagen K, Schomburg D, Rabus R.** 2013. Dynamics of amino acid utilization in *Phaeobacter inhibens* DSM 17395. Proteomics **13:**2869–2885. http://dx.doi.org/10.1002/pmic.201200560.
26. **Drüppel K, Hensler M, Trautwein K, Koßmehl S, Wöhlbrand L, Schmidt-Hohagen K, Ulbrich M, Bergen N, Meier-Kolthoff JP, Göker M, Klenk HP, Schomburg D, Rabus R.** 2014. Pathways and substrate-specific regulation of amino acid degradation in *Phaeobacter inhibens* DSM 17395 (archetype of the marine *Roseobacter* clade). Environ. Microbiol. **16:**218–238. http://dx.doi.org/10.1111/1462-2920.12276.
27. **Gade D, Thiermann J, Markowsky D, Rabus R.** 2003. Evaluation of two-dimensional difference gel electrophoresis for protein profiling. J. Mol. Microbiol. Biotechnol. **5:**240–251. http://dx.doi.org/10.1159/000071076.
28. **Rabus R, Trautwein K.** 2010. Proteogenomics to study the anaerobic degradation of aromatic compounds and hydrocarbons, p 4385–4405. *In* Timmis KN (ed), Handbook of hydrocarbon and lipid microbiology. Springer, Berlin, Germany.
29. **Bradford MM.** 1976. A rapid and sensitive method for the quantification of microgram quantities of protein utilizing the principle of protein-dye binding. Anal. Biochem. **72:**248–254. http://dx.doi.org/10.1016/0003-2697(76)90527-3.
30. **Wöhlbrand L, Kallerhoff B, Lange D, Hufnagel P, Thiermann J, Reinhardt R, Rabus R.** 2007. Functional proteomic view of metabolic regulation in "*Aromatoleum aromaticum*" strain EbN1. Proteomics **7:**2222–2239. http://dx.doi.org/10.1002/pmic.200600987.
31. **Zech H, Echtermeyer C, Wöhlbrand L, Blasius B, Rabus R.** 2011. Biological versus technical variability in 2D DIGE experiments with environmental bacteria. Proteomics **11:**3380–3389. http://dx.doi.org/10.1002/pmic.201100071.
32. **Koßmehl S, Wöhlbrand L, Drüppel K, Feenders C, Blasius B, Rabus R.** 2013. Subcellular protein localization (cell envelope) in *Phaeobacter inhibens* DSM 17395. Proteomics **13:**2743–2760. http://dx.doi.org/10.1002/pmic.201300112.
33. **Oelmüller U, Krüger N, Steinbüchel A, Friedrich CG.** 1990. Isolation of prokaryotic RNA and detection of specific mRNA with biotinylated probes. J. Microbiol. Methods **11:**73–81. http://dx.doi.org/10.1016/0167-7012(90)90050-G.
34. **Kühner S, Wöhlbrand L, Fritz I, Wruck W, Hultschig C, Hufnagel P, Kube M, Reinhardt R, Rabus R.** 2005. Substrate-dependent regulation of anaerobic degradation pathways for toluene and ethylbenzene in a denitrifying bacterium, strain EbN1. J. Bacteriol. **187:**1493–1503. http://dx.doi.org/10.1128/JB.187.4.1493-1503.2005.
35. **Caspi R, Altman T, Dreher K, Fulcher CA, Subhraveti P, Keseler IM, Kothari A, Krummenacker M, Latendresse M, Mueller LA, Ong Q, Paley S, Pujar A, Shearer AG, Travers M, Weerasinghe D, Zhang P, Karp PD.** 2012. The MetaCyc database of metabolic pathways and enzymes and the BioCyc collection of pathway/genome databases. Nucleic Acids Res. **40:**D742–D753. http://dx.doi.org/10.1093/nar/gkr1014.
36. **Kanehisa M, Goto S, Sato Y, Furumichi M, Tanabe M.** 2012. KEGG for integration and interpretation of large-scale molecular data sets. Nucleic Acids Res. **40:**D109–D114. http://dx.doi.org/10.1093/nar/gkr988.
37. **Rutherford K, Parkhill J, Crook J, Horsnell T, Rice P, Rajandream MA, Barrel B.** 2000. Artemis: sequence visualization and annotation. Bioinformatics **16:**944–945. http://dx.doi.org/10.1093/bioinformatics/16.10.944.
38. **NCBI Resource Coordinators.** 2013. Database resources of the National Center for Biotechnology Information. Nucleic Acids Res. **41:**D8–D20. http://dx.doi.org/10.1093/nar/gks1189.
39. **Johnson LS, Eddy SR, Portugaly E.** 2010. Hidden Markov model speed heuristic and iterative HMM search procedure. BMC Bioinformatics **11:**431. http://dx.doi.org/10.1186/1471-2105-11-431.
40. **Schomburg I, Chang A, Placzek S, Söhngen C, Rother M, Lang M, Munaretto C, Ulas S, Stelzer M, Scheer M, Schomburg D.** 2013. BRENDA in 2013: integrated reactions, kinetic data, enzyme function data, improved disease classification: new options and contents in BRENDA. Nucleic Acids Res. **41:**D764–D772. http://dx.doi.org/10.1093/nar/gks1049.
41. **UniProt Consortium.** 2012. Reorganizing the protein space at the Universal Protein Resource (UniProt). Nucleic Acids Res. **40:**D71–D75. http://dx.doi.org/10.1093/nar/gkr981.
42. **Goujon M, McWilliam H, Li W, Valentin F, Squizzato S, Paern J, Lopez R.** 2010. A new bioinformatics analysis tools framework at EMBL-EBI. Nucleic Acids Res. **38:**W695–W699. http://dx.doi.org/10.1093/nar/gkq313.
43. **Sievers F, Wilm A, Dineen DG, Gibson TJ, Karplus K, Li W, Lopez R, McWilliam H, Remmert M, Söding J, Thompson JD, Higgins DG.** 2011. Fast, scalable generation of high-quality protein multiple sequence alignments using Clustal Omega. Mol. Syst. Biol. **7:**539. http://dx.doi.org/10.1038/msb.2011.75.
44. **Li L, Stoeckert CJ, Jr, Roos DS.** 2003. OrthoMCL: identification of ortholog groups of eukaryotic genomes. Genome Res. **13:**2178–2189. http://dx.doi.org/10.1101/gr.1224503.
45. **Altschul SF, Gish W, Miller W, Myers EW, Lipman DJ.** 1990. Basic local alignment search tool. J. Mol. Biol. **215:**403–410. http://dx.doi.org/10.1016/S0022-2836(05)80360-2.
46. **Markowitz VM, Chen I, Palaniappan K, Chu K, Szeto E, Grechkin Y, Ratner A, Jacob B, Huang J, Williams P, Huntemann M, Anderson I, Mavromatis K, Ivanova NN, Kyrpides NC.** 2012. IMG: the Integrated Microbial Genomes database and comparative analysis system. Nucleic Acids Res. **40:**D115–D122. http://dx.doi.org/10.1093/nar/gkr1044.
47. **Quester S, Schomburg D.** 2011. EnzymeDetector: an integrated enzyme function prediction tool and database. BMC Bioinformatics **12:**376. http://dx.doi.org/10.1186/1471-2105-12-376.
48. **Benz R.** 1988. Structure and function of porins from Gram-negative bacteria. Annu. Rev. Microbiol. **42:**359–393. http://dx.doi.org/10.1146/annurev.mi.42.100188.002043.
49. **Chen R, Schmidmayr W, Krämer C, Chen-Schmeisser U, Henning U.** 1980. Primary structure of major outer membrane protein II* (*ompA* pro-

tein) of *Escherichia coli* K-12. Proc. Natl. Acad. Sci. U. S. A. **77:**4592–4596. http://dx.doi.org/10.1073/pnas.77.8.4592.
50. **Sugawara E, Nikaido H.** 1994. OmpA protein of *Escherichia coli* outer membrane occurs in open and closed channel forms. J. Biol. Chem. **269:** 17981–17987.
51. **Boulanger A, Déjean G, Lautier M, Glories M, Zischek C, Arlat M, Lauber E.** 2010. Identification and regulation of the *N*-acetylglucosamine utilization pathway of the plant pathogenic bacterium *Xanthomonas campestris* pv. campestris. J. Bacteriol. **192:**1487–1497. http://dx.doi.org/10.1128/JB.01418-09.
52. **Comb DG, Roseman S.** 1958. Glucosamine metabolism. IV. Glucosamine-6-phosphate deaminase. J. Biol. Chem. **232:**807–828.
53. **Badet B, Vermoote P, Haumont PY, Lederer F, Le Goffic F.** 1987. Glucosamine synthetase from *Escherichia coli*: purification, properties, and glutamine-utilizing site location. Biochemistry **26:**1940–1948. http://dx.doi.org/10.1021/bi00381a023.
54. **Cunin R, Glansdorff N, Piérard A, Stalon V.** 1986. Biosynthesis and metabolism of arginine in bacteria. Microbiol. Rev. **50:**314–352.
55. **Lambert A, Østerås M, Mandon K, Poggi M-C, Le Rudulier D.** 2001. Fructose uptake in *Sinorhizobium meliloti* is mediated by a high-affinity ATP-binding cassette transport system. J. Bacteriol. **183:**4709–4717. http://dx.doi.org/10.1128/JB.183.16.4709-4717.2001.
56. **Schneider K-H, Giffhorn F, Kaplan S.** 1993. Cloning, nucleotide sequence and characterization of the mannitol dehydrogenase gene from *Rhodobacter sphaeroides*. J. Gen. Microbiol. **139:**2475–2484. http://dx.doi.org/10.1099/00221287-139-10-2475.
57. **Stein MA, Schäfer A, Giffhorn F.** 1997. Cloning, nucleotide sequence, and overexpression of *smoS*, a component of a novel operon encoding an ABC transporter and polyol dehydrogenases of *Rhodobacter sphaeroides* Si4. J. Bacteriol. **179:**6335–6340.
58. **Willis L, Walker GC.** 1999. A novel *Sinorhizobium meliloti* operon encodes an α-glucosidase and a periplasmic-binding-protein-dependent transport system for α-glucosides. J. Bacteriol. **181:**4176–4184.
59. **Darwin AJ.** 2005. The phage-shock-protein response. Mol. Microbiol. **57:**621–628. http://dx.doi.org/10.1111/j.1365-2958.2005.04694.x.
60. **Model P, Jovanovic G, Dworkin J.** 1997. The *Escherichia coli* phage-shock-protein (*psp*) operon. Mol. Microbiol. **24:**255–261. http://dx.doi.org/10.1046/j.1365-2958.1997.3481712.x.
61. **Shamanna DK, Sanderson KE.** 1979. Uptake and catabolism of D-xylose in *Salmonella typhimurium* LT2. J. Bacteriol. **139:**64–70.
62. **Song S, Park C.** 1997. Organization and regulation of the D-xylose operons in *Escherichia coli* K-12: XylR acts as a transcriptional activator. J. Bacteriol. **179:**7025–7032.
63. **Gade D, Gobom J, Rabus R.** 2005. Proteomic analysis of carbohydrate catabolism and regulation in the marine bacterium *Rhodopirellula baltica*. Proteomics **5:**3672–3683. http://dx.doi.org/10.1002/pmic.200401200.
64. **Barabote RD, Saier MH, Jr.** 2005. Comparative genomic analyses of the bacterial phosphotransferase system. Microbiol. Mol. Biol. Rev. **69:**608–634. http://dx.doi.org/10.1128/MMBR.69.4.608-634.2005.
65. **Higgins CF.** 1992. ABC transporters: from microorganisms to man. Annu. Rev. Cell Biol. **8:**67–113. http://dx.doi.org/10.1146/annurev.cb.08.110192.000435.
66. **Forward JA, Behrendt MC, Wyborn NR, Cross R, Kelly DJ.** 1997. TRAP transporters: a new family of periplasmic solute transport systems encoded by the *dctPQM* genes of *Rhodobacter capsulatus* and by homologs in diverse Gram-negative bacteria. J. Bacteriol. **179:**5482–5493.
67. **Zhao G, Pease AJ, Bharani N, Winkler ME.** 1995. Biochemical characterization of *gapB*-encoded erythrose 4-phosphate dehydrogenase of *Escherichia coli* K-12 and its possible role in pyridoxal 5′-phosphate biosynthesis. J. Bacteriol. **177:**2804–2812.
68. **Helsper JP, Loewus FA.** 1982. Metabolism of L-threonic acid in *Rumex x acutus* L. and *Pelargonium crispum* (L.) L'Hér. Plant Physiol. **69:**1365–1368. http://dx.doi.org/10.1104/pp.69.6.1365.
69. **Riemer AS, Rex R, Schomburg D.** 2013. A metabolite-centric view on flux distributions in genome-scale metabolic models. BMC Syst. Biol. **7:**33. http://dx.doi.org/10.1186/1752-0509-7-33.
70. **Jackson JB.** 2003. Proton translocation by transhydrogenase. FEBS Lett. **545:**18–21. http://dx.doi.org/10.1016/S0014-5793(03)00388-0.
71. **Newton RJ, Griffin LE, Bowles KM, Meile C, Gifford S, Givens CE, Howard EC, King E, Oakley CA, Reisch CR, Rinta-Kanto JM, Sharma S, Sun S, Varaljay V, Vila-Costa M, Westrich JR, Moran MA.** 2010. Genome characteristics of a generalist marine bacterial lineage. ISME J. **4:**784–798. http://dx.doi.org/10.1038/ismej.2009.150.